PCCP

ROYAL SOCIETY OF CHEMISTRY

PAPER

View Article Online
View Journal | View Issue

Cite this: *Phys. Chem. Chem. Phys.*, 2021, **23**, 5460

Low lattice thermal conductivity of a 5–8-peanut-shaped carbon nanotube†

Jie Sun, Yanyan Chen and Qian Wang *

Received 10th December 2020,
Accepted 6th February 2021

DOI: 10.1039/d0cp06390h

rsc.li/pccp

5–8-defects are well-known in graphene and other 2D carbon structures, but not well-studied in one dimensional (1D) carbon materials. Here, we design a peanut-shaped carbon nanotube by assembling the 5–8-cage composed of carbon 5- and 8-membered rings, named 5–8-PSNT. Using first-principles calculations and molecular dynamics simulations, we find that 5–8-PSNT is not only thermally and dynamically stable, but also metallic. Moreover, its lattice thermal conductivity is only 95.87 W m^{-1} K^{-1}, which is less than one tenth of the value of (6, 6) carbon nanotube that has a radius similar to that of 5–8-PSNT. A further analysis of the phonon properties reveals that the low lattice thermal conductivity of 5–8-PSNT arises from its low phonon group velocity, short relaxation time, large lattice vibrational mismatch and strong anharmonicity. These findings further suggest that a pentagon and an octagon as structural units can effectively modulate the properties of carbon materials.

1. Introduction

Since the experimental observation of a 1D topological defect composed of pentagonal and octagonal sp^2-hybridized carbon rings in graphene,[1] carbon materials containing such 5–8 defects have attracted much attention. For example, it was found that zigzag graphene nanoribbons (GNRs) are antiferromagnetic in cross-edge coupling, which can be switched to ferromagnetic coupling when 5–8 topological line defects are introduced.[2] Similarly, the electronic structure and magnetic properties of armchair GNRs can be effectively tuned by 5–8 topological line defects.[3] Recently, it has been reported that 5–8 defects can significantly affect the thermal transport properties of carbon materials and reduce their lattice thermal conductivity. For instance, Yousefi *et al.*[4] performed molecular dynamics calculations and found that the thermal conductivity of carbon nanotubes (CNTs) with 5–8 defects reduces because of the enhanced phonon scattering. Luo *et al.*[5] reported the sensitivity of the thermal conductance of GNRs with 5–8 defects to the defect configurations. Fthenakis *et al.*[6] found that the existence of 5–8 defects in graphene makes the thermal conductivity anisotropic and quenches its value by one to two orders of magnitude, as compared to the pristine graphene due to the reduction of the phonon mean free path.

However, for all the reported 1D carbon structures so far, the 5–8 unit is treated as a defect, where the C atoms are in sp^2 bonding. It would be interesting and highly desirable to design new 1D carbon structures composed entirely of 5–8 units and containing sp^3 bonding because some exceptional properties can be expected according to the property–structure relationship. As is well known, the lattice thermal conductivity of a material is an important physical quantity that characterizes the thermal transport properties, which can be determined by the following factors: the average atomic mass, complexity of the geometry, strength of the interatomic bonding and degree of the lattice anharmonicity.[7] Low lattice thermal conductivity is essential to achieve high performance for thermoelectric materials. However, for some materials with light atoms, like CNTs and graphene, it is difficult to achieve low thermal conductivity because of their large phonon group velocity and mean free path, and thus their intrinsic lattice thermal conductivities are usually quite high and can reach 3000 W m^{-1} K^{-1}.[8] As stated above, the structures containing the 5–8 units can have much lower lattice thermal conductivity than their hexagonal counterparts. Therefore, we are curious about how high the lattice thermal conductivity of a 1D carbon structure composed of pure 5–8 units is, which motivates us to carry out this study by using first principles calculations combined with non-equilibrium molecular dynamics simulations.

2. Computational methods

Geometry optimization and electronic structure are calculated within the framework of density functional theory (DFT) and the projector augmented wave (PAW) method[9] implemented in the Vienna *Ab initio* Simulation Package (VASP) is used.[10,11] The

Center for Applied Physics and Technology, HEDPS, College of Engineering, and School of Materials Science and Engineering, BKL-MEMD, Peking University, Beijing 100871, China. E-mail: qianwang2@pku.edu.cn

† Electronic supplementary information (ESI) available. See DOI: 10.1039/d0cp06390h

Perdew–Burke–Ernzerhof (PBE) functional[12] within the generalized gradient approximation (GGA)[13] is used to treat the electronic exchange–correlation interaction. The energy cutoff is set to 500 eV and a 9 × 9 × 1 Monkhorst–Pack K point mesh[14] is adopted to sample the Brillouin zone in reciprocal space. The convergence of criteria for the force and energy components is set to 10^{-2} eV Å^{-1} and 10^{-4} eV, respectively. A vacuum space of 15 Å is set along the transverse directions of the structures.

The spectral energy density (SED) method[15] is used to calculate the phonon relaxation time.[16,17] The phonon normal modes can be obtained using the following equation:

$$Q(\boldsymbol{k},\mu,t)=\sum_{ji}\sqrt{\frac{m_j}{N}}\boldsymbol{v}_{ji}\cdot\boldsymbol{e}_j(\boldsymbol{k},\mu)\exp(-2\pi i\boldsymbol{k}\cdot\boldsymbol{r}_l) \quad (1)$$

where $\boldsymbol{k}$, μ, and m_j are the wave factor, phonon branch and the mass of jth atom, respectively, N is the number of unit cell, $\boldsymbol{v}_{jl}$ represents the velocity of jth atom in the lth unit cell, and $\boldsymbol{e}_j$ is the eigenvector of jth phonon mode. Then, the spectral energy density can be calculated by taking Fourier transform using the equation:

$$\Phi(\boldsymbol{k},\mu,f)=\left|\int Q(\boldsymbol{k},\mu,t)\exp(-2\pi ift)\mathrm{d}t\right|^2 \quad (2)$$

In addition, the spectral energy density can also be obtained by:

$$\Phi(\boldsymbol{k},\mu,f)=\frac{I}{1+[2\pi[f-f_0(\boldsymbol{k},\mu)]/\Gamma(\boldsymbol{k},\mu)]^2} \quad (3)$$

where I represents the peak magnitude, $f_0(\boldsymbol{k},\mu)$ is frequency at the peak center, and $\Gamma(\boldsymbol{k},\mu)$ is the half-width at half-maximum. The phonon relaxation time can be calculated by fitting the following function: $\tau(\boldsymbol{k},\mu)=1/2\Gamma(\boldsymbol{k},\mu)$.

The thermal conductivity is calculated using non-equilibrium molecular dynamics (NEMD) method as implemented in the large-scale atomic/molecular massively parallel simulation (LAMMPS).[18] We set fixed walls at the ends of structures and control the temperature by subtracting/adding heat at the heat sink/reservoir. Each structure is divided into 25 slabs. The simulation time step is set to 0.25 fs and a vacuum space is set along the transverse directions to avoid the interactions. The structures are first relaxed in *NPT* and *NVT* ensemble for 10^7 steps, respectively, and then thermalized in *NVE* ensemble for another 10^7 steps to reach a steady state. The thermal conductivity is calculated by using Fourier's law: $k=J/\nabla T$, where J is the heat flux and ∇T is the temperature gradient. The Tersoff potential proposed by Lindsay and Broido[19] is used to describe the interatomic interactions of carbon atoms, which has been proved successfully to calculate the thermal conductivity of CNTs and graphene in previous studies.[20,21] In addition, we calculate the C–C bond lengths in 5–8-PSNT with the Tersoff potential using MD simulation and compare the results with those of DFT calculations. After geometry optimization, the corresponding bond lengths are found to be close to each other, suggesting the accuracy of the Tersoff potential for describing the carbon–carbon interactions in 5–8-PSNT. The details can be found in Fig. S1 in the ESI.†

3. Results and discussions

3.1. Geometry and band structure

We first construct a 5–8 cage structure by using 24 carbon pentagons and 6 octagons, as shown in Fig. 1(a) and (b), similar to a zero-dimensional fullerene. Motivated by the recent experiment of realizing the precise dimerization of hollow fullerene compartments[22] and the previous work on the synthesis of peanut-shaped CNTs by using C_{60} fullerene as the structural unit,[23] we connect two 5–8 cages *via* four carbon atoms, forming the structure unit of a 1D CNT with different curvatures. Due to the composition of pentagons and octagons, as shown in Fig. 1(c–e), we name this new peanut-shaped CNT 5–8-PSNT. The structure unit contains 120 carbon atoms, and the lattice constant along the a (longitudinal) direction is 18.61 Å. The cross sectional area is needed to calculate the heat flux through the structure and the lattice thermal conductivity. The cross section of (6,6) CNT can be seen as circles with the same diameter. For 5–8-PSNT, the cross section is not uniform but can be treated as circles with different diameters. Here, the distance between the highest and lowest atoms d_{max} as indicated in Fig. 1(e) is 6.42 Å, which is chosen as the diameter of 5–8-PSNT. Considering the van der Waals radius (3.4 Å),[24] the physical diameters used to calculate the cross sectional areas for 5–8-PSNT and (6,6) CNT are 9.82 and 11.47 Å, respectively.

We then check the stability of 5–8-PSNT. The structure is first thermalized in the *NPT* ensemble for 2500 ps at 1000 K by using the molecular dynamics. It is found that 5–8-PSNT can keep its original geometry and nearly constant energy during the relaxation, as shown in Fig. 2(a), confirming the thermal stability of this structure. The phonon dispersion of 5–8-PSNT is calculated using molecular dynamics and plotted in Fig. 2(b). No imaginary mode is found in the phonon spectrum, suggesting

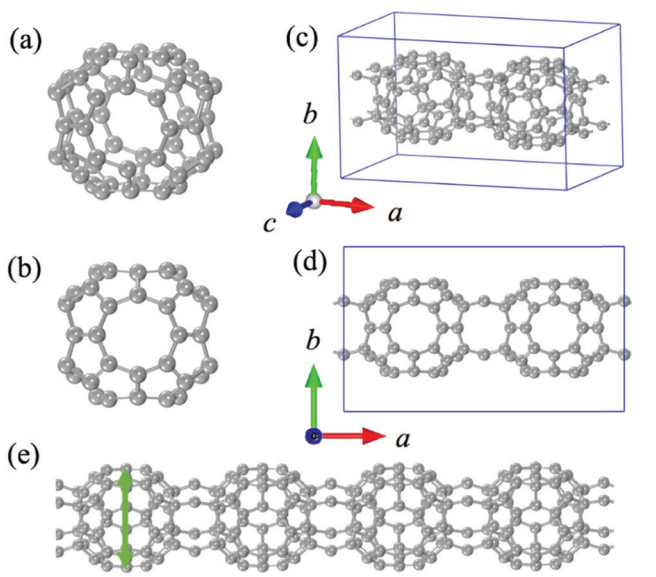

Fig. 1 (a and b) Side and top views of 5–8 cage structure constructed by using pentagons and octagons. (c and d) Side and top views of the structural unit of 5–8-PSNT. (e) Geometric structure of 5–8-PSNT.

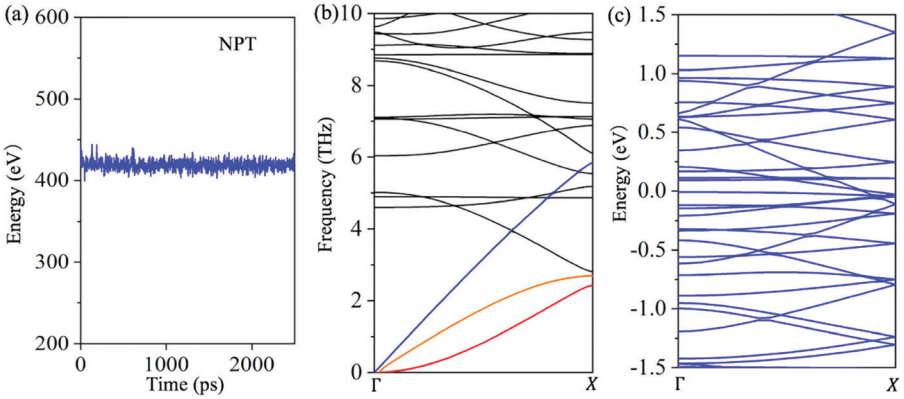

Fig. 2 (a) Variation of the energy with simulation time in the *NPT* ensemble for 5–8-PSNT at 1000 K. (b) Phonon dispersion, and (c) band structure of 5–8-PSNT.

the dynamical stability of 5–8-PSNT. Besides, we note that all the three acoustic phonon branches (marked in red, orange and blue) exhibit frequencies lower than 6 THz, indicating a possible low phonon group velocity and low lattice thermal conductivity.

We next study the electronic band structure of 5–8-PSNT. The calculated results are plotted in Fig. 2(c), which shows metallic behavior as the partially occupied bands cross the Fermi level, similar to the case of armchair (m, m) CNTs, although their geometric features are very different, namely, there is no hexagon in 5–8-PSNT while the armchair CNT is composed entirely of hexagons, suggesting that the metallicity in 1D carbon structures can be induced either by changing the chirality or by introducing 5- and 8-membered rings.

3.2. Lattice thermal conductivity

To obtain the lattice thermal conductivity, the temperature gradient developed when the heat flux travels through structures is first calculated. Here, we take the length of 50 nm as an example. To have a comparison with the conventional CNTs, we choose (6, 6) CNT that is also metallic with a similar radius to that of 5–8-PSNT. The results are shown in Fig. 3(a). One can see that the temperature distributions in 5–8-PSNT and (6, 6) CNT both have linear characteristics along the heat transfer directions, indicating that the parameters set in the simulations are appropriate. The nonlinear parts of the distribution at the heat reservoir and sink are caused by the edge effects. To avoid the edge effects, only the linear parts are taken to calculate the temperature gradient.

In NEMD simulations, the thermal conductivities become larger as the size increases[25,26] due to the size effect where phonon propagation can be affected by the edges when the phonon mean free path (MFP) is larger than the length of the simulation structure. The size effect can be eliminated when the length of the structure is much larger than the phonon MFP, and in this case, the thermal conductivity can eventually converge to a constant value.[27] Therefore, we choose some specific lengths (50, 100, 200, 300, 500, 800 and 1000 nm) to calculate the thermal conductivities for both 5–8-PSNT and (6, 6) CNT, as shown in Fig. 3(b). The thermal conductivities with error bars are plotted in Fig. S2 in the ESI.† The average lattice thermal conductivities of 5–8-PSNT are calculated to be 14.38, 18.25, 32.13, 44.80, 59.15, 93.95 and 95.87 W m^{-1} K^{-1} for lengths of 50, 100, 200, 300, 500, 800 and 1000 nm, respectively, much lower than 318.31, 515.63, 659.55, 764.48, 857.33, 941.45 and 994.99 W m^{-1} K^{-1} for the corresponding lengths of (6,6) CNT. The calculated thermal conductivities of (6,6) CNT are consistent with previous studies.[28,29] In low-dimensional systems, the thermal conductivity (κ) of a material depends on its length (L) with a relationship of $\kappa \sim L^{\alpha}$, $\alpha > 0$. For instance, for CNTs and silicon nanowires, the heat transfer shows power-law

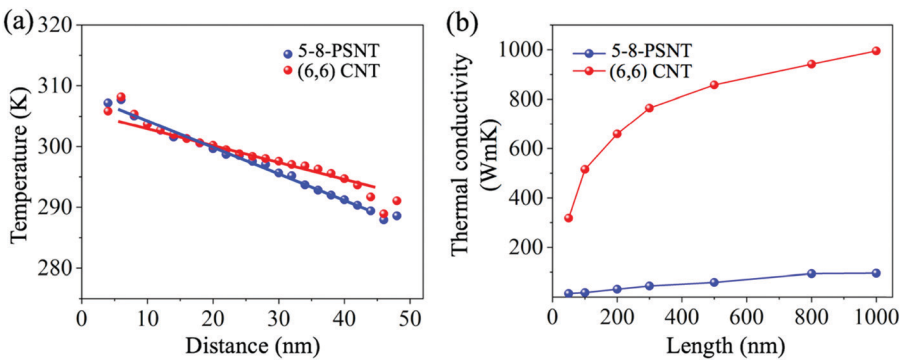

Fig. 3 (a) Temperature profile, and (b) variation of the average thermal conductivity with the length for 5–8-PSNT and (6,6) CNT.

divergence ($\alpha < 1$).[30] According to the calculated lattice thermal conductivities of 5–8-PSNT with different lengths, the value of α is 0.68, smaller than 1. Therefore, a power-law divergence of thermal conductivity with length is also suitable for 5–8-PSNT structure.

It is exciting to find that the lattice thermal conductivity of this new 1D peanut-shaped carbon nanotube is less than one tenth of that of (6,6) CNT, indicating a promising application of this carbon allotrope in the field where low lattice thermal conductivity is required. For both structures, the increase of lattice thermal conductivity with the length becomes slower as the edge effect becomes less dominant at large size. The eventual lattice thermal conductivity of 5–8-PSNT converges to 93.95 W m^{-1} K^{-1} at 800 nm, while for (6,6) CNT, the lattice thermal conductivity still has the increasing trend even when the simulation size has reached 1000 nm. The temperature dependence of the lattice thermal conductivity for 5–8-PSNT (50 nm) is calculated and plotted in Fig. S3 in the ESI.† The average lattice thermal conductivities of 5–8-PSNT are found to be 23.89, 19.09, 14.38, 6.08 1.99 and 1.40 W m^{-1} K^{-1} for temperatures of 100, 200, 300, 400, 500 and 600 K, respectively. One can see that the thermal conductivity decreases with temperature which can be attributed to more phonon scattering at higher temperatures.

3.3. Phonon properties

To understand why the lattice thermal conductivity of 5–8-PSNT is much lower than that of (6,6) CNT, we calculate the phonon group velocities and relaxation time as shown in Fig. 4, showing that the phonon group velocities of 5–8-PSNT are smaller than those of (6, 6) CNT in the entire frequency region and the average group velocity of 5–8-PSNT is 11.12 m s^{-1}, only one fifth of the value of the (6,6) CNT (57.83 m s^{-1}). We further calculate the average phonon group velocity of the low frequency region (0–5 THz), middle frequency region (5–40 THz) and high frequency region, respectively, to see the difference more clearly. The corresponding average phonon group velocities for 5–8-PSNT are 44.93, 11.66 and 1.57 m s^{-1}, while the corresponding values for (6, 6) CNT are 68.35, 57.83 and 23.87 m s^{-1}, respectively. One can see that the phonon group velocities for the two structures both decrease as the frequencies increase since the acoustic phonon branches usually dominate the thermal transport. It is observed that the differences in phonon group velocities are mainly reflected in the middle and high frequency ranges. For instance, the average phonon group velocity of (6, 6) CNT (23.87 m s^{-1}) with high frequencies is more than ten times larger than that of 5–8-PSNT (1.57 m s^{-1}). Fig. 4(b) shows that the phonon relaxation time of 5–8-PSNT is also much less than that of (6, 6) CNT in the whole frequency region. In the low, middle and high frequency regions, the corresponding phonon relaxation time for 5–8-PSNT is 18.45, 1.34 and 0.51 ps, while those values for (6, 6) CNT are 30.01, 5.04 and 1.58 ps, respectively. The reduced phonon group velocities, combined with phonon relaxation time, directly lead to the low lattice thermal conductivity of 5–8-PSNT.

3.4. Vibrational mismatch

It is known that the phonon transport in a structure is actually the transport of lattice vibrations and the lattice thermal transport is the whole behavior of lattice vibrations. Previous studies have shown that the thermal transport can be hindered if the lattice vibrations of different regions in a structure are different from each other.[31,32] and the larger difference would lead to the lower thermal conductivity. The lattice vibrations are usually characterized by the vibrational density of states (VDOS), which describes the frequency distributions of phonons by taking Fourier transform on the atom velocity autocorrelation function.[31,33] Two different regions in 5–8-PSNT and (6,6) CNT (see Fig. 5(a) and (b)) are chosen to calculate their VDOS and the results are shown in Fig. 5(c) and (d). It is found that, for 5–8-PSNT, the VDOS of region 1 has an obvious deviation from the VDOS of region 2 in many frequency regions, whereas the VDOS of two regions are nearly overlapped together in the CNT. To quantify the overlap between the two regions, we integrate the vibrational spectra over frequency by using the equation:[34,35] $I = \int f_1(\omega) f_2(\omega) d\omega$, where $f_1(\omega)$ and $f_2(\omega)$ are the spectral functions of phonon mode frequency ω of the two regions. Based on the above relation, the calculated result for 5–8-PSNT is 0.10 and the value for (6,6) CNT is 0.13, increased by 30 percent. The less overlap of the vibrations in 5–8-PSNT indicates that the phonons would be hindered more due to the larger lattice vibrational

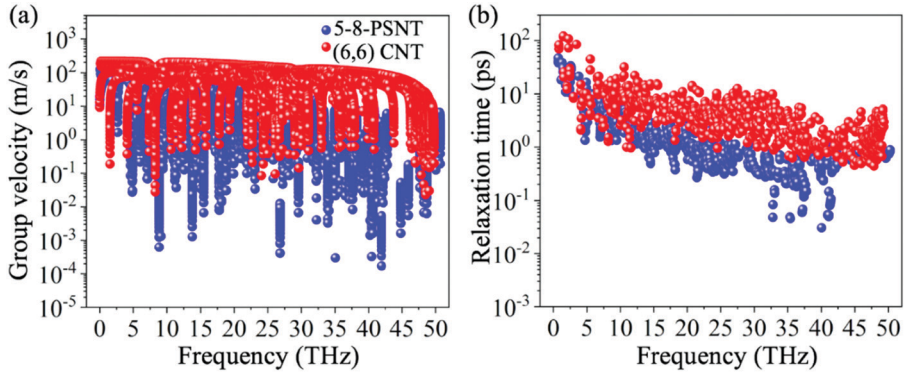

Fig. 4 (a) Group velocity and (b) phonon relaxation time *versus* frequency for 5–8-PSNT and (6, 6) CNT.

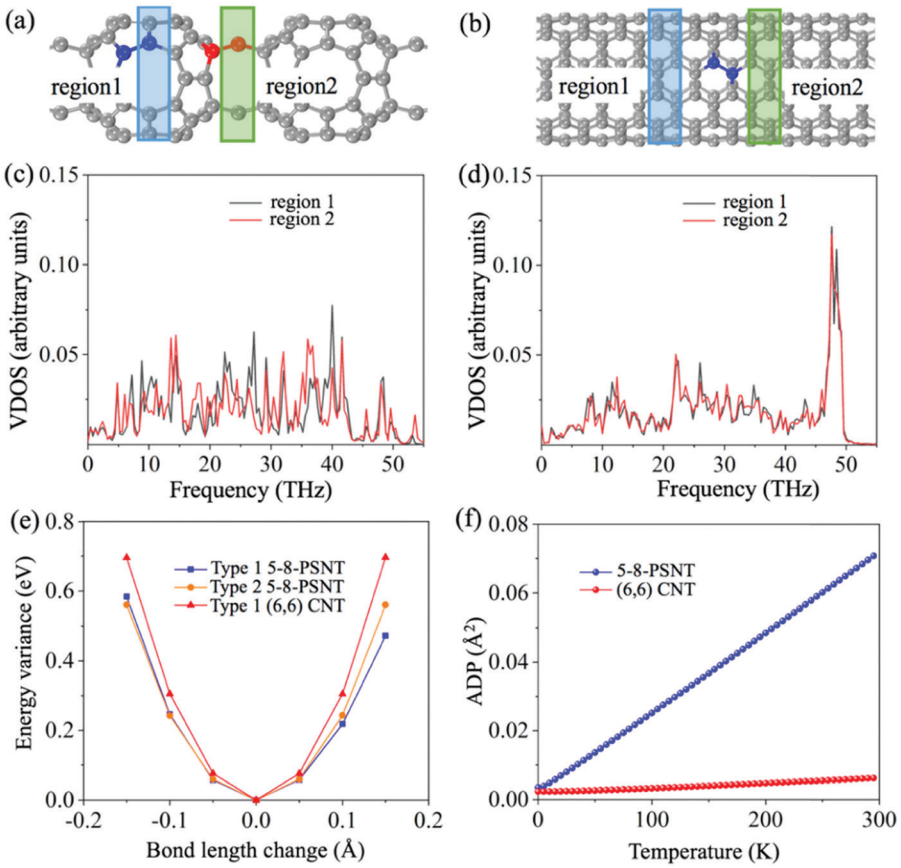

Fig. 5 (a and b) Schematic diagrams of the two regions, and (c and d) VDOS for 5–8-PSNT and (6, 6) CNT. (c and d) Energy variance as a function of bond length change and ADP as a function of temperature for 5–8-PSNT and (6,6) CNT.

mismatch, thus leading to its low lattice thermal conductivity. Interestingly, a recent work found that the vibrational hierarchy in a crystal can be a key factor leading to the low lattice thermal conductivity.[36] The different vibrational modes in two regions is similar to the hierarchy phonon transport as in a previous work, further confirming the low lattice thermal conductivity of 5–8-PSNT.

3.5. Anharmonicity

The anharmonicity of a structure is the underlying factor determining the phonon properties and the thermal conductivity. Large anharmonicity, indicating a strong phonon scattering, usually leads to the low lattice thermal conductivity. Generally, the whole lattice anharmonicity depends on the bond anharmonicity in a structure. To illustrate the bond anharmonicity, the energy profiles as a function of the bond length of 5–8-PSNT and (6,6) CNT are calculated. For 5–8-PSNT, we choose two types of C–C bonds to do the calculation, with one existing in the cage forming pentagonal rings (marked in blue in Fig. 5(a)) and another localizing in the middle connecting the cages together (marked in red in Fig. 5(a)). For (6, 6) CNT, we choose the C–C bond marked in blue as shown in Fig. 5(b) to do the calculation. The energies are calculated by compressing and stretching the bonds away from their equilibrium positions along the longitudinal direction and the calculated results are shown in Fig. 5(e). It is known that the deviation of the bond energy profile from the quadratic profile can depict the bond anharmonicity.[37] Therefore, we fit the energy profiles of the bonds using quadratic polynomial. The harmonic fit equations of the energy variance curves for the type 1 and 2 bonds in 5–8-PSNT and the type 1 bond in (6,6) CNT are: $y = 23.51x^2 - 0.28x$, $y = 24.99x^2 + 0.01x$ and $y = 30.98x^2 + 0.01x$, respectively. One can note that the quadratic parameter of the energy profile for the type 1 (type 2) bond in 5–8-PSNT is about 23.51 (24.99), smaller than that for (6,6) CNT (30.98), indicating the larger lattice anharmonicity in 5–8-PSNT.

The atomic displacement parameter (ADP) can describe the average displacements of atoms vibrating from their equilibrium positions and can reflect the strength of the chemical bond. A relatively small ADP usually indicates that the atoms vibrate less frequently from the equilibrium positions, and in that case, atoms are constrained by a large restoring force, implying a large harmonicity and high lattice thermal conductivity. Here, as shown in Fig. 5(f), the ADP for 5–8-PSNT is 0.071, more than ten times larger than that of (6,6) CNT, the value of which is only 0.006. Such a huge difference in ADP can also account for the large anharmonicity and low lattice thermal conductivity of 5–8-PSNT.

To further explore the origins of the anharmonicity of the two structures, the electronic localization function (ELF) is calculated,[38] which can directly picture the electron configuration, by using the equation: $\mathrm{ELF} = 1/([1 + [K(\boldsymbol{r})/K_h(\boldsymbol{r})]^2])$, where $K(\boldsymbol{r})$ is the curvature of the pair electron density for the actual system at the

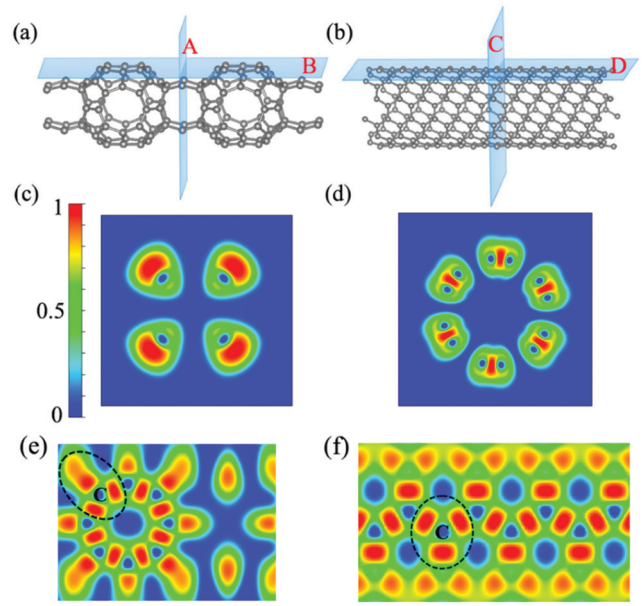

Fig. 6 Schematic of the typical cross section and tangent plane on (a) 5–8-PSNT and (b) (6,6) CNT. ELF of 5–8-PSNT and (6,6) CNT in (c and d) the cross section, and (e) and (f) the tangent plane, respectively.

location $\boldsymbol{r}$, and $K_h(\boldsymbol{r})$ represents the counterpart of a homogeneous electron gas with the same density at the same location. The value of the ELF ranges from 0 to 1. ELF = 0.5 means that the electrons are highly delocalized and ELF = 1 implies the full localization of electrons. Fig. 6(a) and (b) show the cross sections and tangent planes of the 2D ELF, in 5–8-PSNT and (6,6) CNT. Planes A and B in 5–8-PSNT contain carbon atoms at the cage part along the transverse direction and atoms in the connection part along the longitudinal direction, respectively. Planes C and D in (6,6) CNT are perpendicular and parallel to the longitudinal direction, respectively. The 2D ELF of plane A in Fig. 6(c) shows that the lone-pair electrons exist around the carbon atoms at the connection part of 5–8-PSNT. Previous studies have shown that the existence of lone-pair electrons can have strong interaction with the phonons during the heat transport, thus leading to the low lattice thermal conductivity.[39–43] The lone-pair electrons in this new carbon allotrope can contribute to its strong anharmonicity and thus reduce the lattice thermal conductivity. However, one can see that no lone-pair electrons appear in (6,6) CNT (see Fig. 6(d)). Fig. 6(e) and (f) shows the 2D ELF of planes B and D in the two structures. It is observed that the electrons in 5–8-PSNT distribute more inhomogeneously in the cage part than the distribution of electrons in (6,6) CNT. We can see that there are three σ bonds around a carbon atom in both structures. For 5–8-PSNT, the electron distributions from the three regions around the atom are not symmetric (see the black circle in Fig. 6(e)), due to the unique geometry of the structure. The asymmetric nonlinear electrostatic force induced by the neighboring electrons on the atoms in 5–8-PSNT can enhance the anharmonicity and thus reduce the lattice thermal conductivity. However, for (6,6) CNT, the three σ bonds are more symmetric, implying a more homogeneous electrostatic force on the atoms, leading to its strong harmonicity and high thermal conductivity. The asymmetric electron distributions and the existence of lone-pair electrons synergistically give rise to strong anharmonicity of 5–8-PSNT and thus relatively low lattice thermal conductivity, which can be a guiding strategy to design materials with low lattice thermal conductivity.

4. Conclusions

In this work, we design a new 1D carbon allotrope composed entirely of 5–8-units, 5–8-PSNT, which is confirmed to be thermally and dynamically stable. Based on first-principles calculations and molecular dynamics simulations, the thermal transport properties of 5–8-PSNT are studied systematically. Its lattice thermal conductivity is calculated to be 95.87 W m^{-1} K^{-1}, which is much less than that of (6, 6) CNT (994.99 W m^{-1} K^{-1} at 1000 nm). The exhibited low lattice thermal conductivity of 5–8-PSNT can be attributed to the following factors: (1) low phonon group velocity and short relaxation time; (2) large vibrational mismatch of the lattice; and (3) strong anharmonicity induced by unique geometry and the lone-pair electrons. These findings demonstrate that the thermal conductivity of 1D carbon-based materials can be modulated effectively by changing their structure unit and geometry, and 5–8-PSNT expands the family of carbon containing pentagonal and octagonal units with new features.

Conflicts of interest

There are no conflicts to declare.

Acknowledgements

This work is partially supported by grants from the National Key Research and Development Program of the Ministry of Science and technology of China (Grant No. 2017YFA0205003) and the National Science Foundation of China (Grants No. NSFC-11974028 and NSFC-21773004), and is supported by the High-Performance Computing Platform of Peking University, China. Jie Sun thanks Dr Kunpeng Yuan for the useful discussion about using the SED method to calculate the phonon relaxation time.

References

1 J. Lahiri, Y. Lin, P. Bozkurt, I. I. Oleynik and M. Batzill, *Nat. Nanotechnol.*, 2010, **5**, 326.
2 Q. Dai, Y. Zhu and Q. Jiang, *Phys. Chem. Chem. Phys.*, 2014, **16**, 10607–10613.
3 L. Han and Q. Dai, *Chem. Phys. Lett.*, 2015, **623**, 60–67.
4 F. Yousefi and F. Khoeini, *AIP Adv.*, 2019, **9**, 025024.
5 M. Luo, B.-L. Li and D. Li, *Nanomaterials*, 2019, **9**, 1609.
6 Z. G. Fthenakis, Z. Zhu and D. Tománek, *Phys. Rev. B: Condens. Matter Mater. Phys.*, 2014, **89**, 125421.
7 Y. Shen, F. Q. Wang and Q. Wang, *Nano Energy*, 2020, 104822.

8 A. Dey, O. P. Bajpai, A. K. Sikder, S. Chattopadhyay and M. A. S. Khan, *Renewable Sustainable Energy Rev.*, 2016, **53**, 653–671.
9 P. E. Blöchl, *Phys. Rev. B: Condens. Matter Mater. Phys.*, 1994, **50**, 17953–17979.
10 G. Kresse and J. Furthmüller, *Phys. Rev. B: Condens. Matter Mater. Phys.*, 1996, **54**, 11169–11186.
11 G. Kresse and J. Furthmüller, *Comput. Mater. Sci.*, 1996, **6**, 15–50.
12 J. P. Perdew, K. Burke and M. Ernzerhof, *Phys. Rev. Lett.*, 1996, **77**, 3865–3868.
13 Y. Liu and C. Storey, *J. Optim. Theor. Appl.*, 1991, **69**, 129–137.
14 H. J. Monkhorst and J. D. Pack, *Phys. Rev. B: Solid State*, 1976, **13**, 5188–5192.
15 J. Larkin, J. Turney, A. Massicotte, C. Amon and A. McGaughey, *J. Comput. Theor. Nanosci.*, 2014, **11**, 249–256.
16 Y. Zhou, X. Zhang and M. Hu, *Phys. Rev. B: Condens. Matter Mater. Phys.*, 2015, **92**, 195204.
17 X. Zhang, H. Bao and M. Hu, *Nanoscale*, 2015, **7**, 6014–6022.
18 S. Plimpton, *J. Comput. Phys.*, 1995, **117**, 1–19.
19 L. Lindsay and D. Broido, *Phys. Rev. B: Condens. Matter Mater. Phys.*, 2010, **81**, 205441.
20 A. Bagri, S.-P. Kim, R. S. Ruoff and V. B. Shenoy, *Nano Lett.*, 2011, **11**, 3917–3921.
21 K. Sääskilahti, J. Oksanen, S. Volz and J. Tulkki, *Phys. Rev. B: Condens. Matter Mater. Phys.*, 2015, **91**, 115426.
22 F. Han, R. Wang, B. Chen, Y. Feng, H. Liu, S. Wang, D. Su, H. Zhang and H. Chen, *J. Am. Chem. Soc.*, 2020, **142**, 15396–15402.
23 A. Takashima, T. Nishii and J. Onoe, *J. Phys. D: Appl. Phys.*, 2012, **45**, 485302.
24 W. Xu, G. Zhang and B. Li, *J. Chem. Phys.*, 2015, **143**, 154703.
25 C. Oligschleger and J. Schön, *Phys. Rev. B: Condens. Matter Mater. Phys.*, 1999, **59**, 4125.
26 R. H. Poetzsch and H. Böttger, *Phys. Rev. B: Condens. Matter Mater. Phys.*, 1994, **50**, 15757.
27 D. P. Sellan, E. S. Landry, J. Turney, A. J. McGaughey and C. H. Amon, *Phys. Rev. B: Condens. Matter Mater. Phys.*, 2010, **81**, 214305.
28 M. Alaghemandi, E. Algaer, M. C. Böhm and F. Müller-Plathe, *Nanotechnology*, 2009, **20**, 115704.
29 Z. Han and A. Fina, *Prog. Polym. Sci.*, 2011, **36**, 914–944.
30 V. Lee, C.-H. Wu, Z.-X. Lou, W.-L. Lee and C.-W. Chang, *Phys. Rev. Lett.*, 2017, **118**, 135901.
31 M. Hu, Y. Jing and X. Zhang, *Phys. Rev. B: Condens. Matter Mater. Phys.*, 2015, **91**, 155408.
32 J. Sun, K. Yuan, W. Zhou, X. Zhang, J. Onoe, Y. Kawazoe and Q. Wang, *Nanotechnology*, 2019, **31**, 115701.
33 W. He, D. Wang, H. Wu, Y. Xiao, Y. Zhang, D. He, Y. Feng, Y.-J. Hao, J.-F. Dong and R. Chetty, *Science*, 2019, **365**, 1418–1424.
34 Y. Wang, Y. Cao, K. Zhou and Z. Xu, *Adv. Mater. Interfaces*, 2017, **4**, 1700355.
35 H. Chen, Y. Cao, J. Zhang and C. Zhou, *Nat. Commun.*, 2014, **5**, 1–12.
36 Y. Luo, X. Yang, T. Feng, J. Wang and X. Ruan, *Nat. Commun.*, 2020, **11**, 1–10.
37 X. Wu, V. Varshney, J. Lee, T. Zhang, J. L. Wohlwend, A. K. Roy and T. Luo, *Nano Lett.*, 2016, **16**, 3925–3935.
38 A. D. Becke and K. E. Edgecombe, *J. Chem. Phys.*, 1990, **92**, 5397–5403.
39 E. J. Skoug and D. T. Morelli, *Phys. Rev. Lett.*, 2011, **107**, 235901.
40 M. D. Nielsen, V. Ozolins and J. P. Heremans, *Energy Environ. Sci.*, 2013, **6**, 570–578.
41 B. Du, R. Zhang, K. Chen, A. Mahajan and M. J. Reece, *J. Mater. Chem. A*, 2017, **5**, 3249–3259.
42 M. K. Jana, K. Pal, U. V. Waghmare and K. Biswas, *Angew. Chem.*, 2016, **128**, 7923–7927.
43 E. Rathore, R. Juneja, S. P. Culver, N. Minafra, A. K. Singh, W. G. Zeier and K. Biswas, *Chem. Mater.*, 2019, **31**, 2106–2113.

